Composites Part B 122 (2017) 16–22

Contents lists available at ScienceDirect

Composites Part B

journal homepage: www.elsevier.com/locate/compositesb

Influence of aramid fiber treatment and carbon nanotubes on the interfacial strength of polypropylene hierarchical composites

P.I. Gonzalez-Chi [a], O. Rodríguez-Uicab [a], C. Martin-Barrera [a], J. Uribe-Calderon [a, *], G. Canché-Escamilla [a], M. Yazdani-Pedram [b], A. May-Pat [a], F. Avilés [a]

[a] Centro de Investigación Científica de Yucatán A.C., Unidad de Materiales, Calle 43 No.130 x 32 y 34, Col. Chuburna de Hidalgo, C.P. 97205, Mérida, Yucatán, Mexico

[b] Facultad de Ciencias Químicas y Farmacéuticas, Universidad de Chile, S. Livingstone 1007, Independencia, Santiago, Chile

ARTICLE INFO

Article history:
Received 7 January 2017
Received in revised form
5 April 2017
Accepted 8 April 2017
Available online 11 April 2017

Keywords:
Interface/interphase
Aramid fiber
Surface properties
Nano-structures
Micro-mechanics

ABSTRACT

The microbond test was used to evaluate the interfacial shear strength (IFSS) of multiscale composites based on a polypropylene (PP) matrix reinforced with aramid fibers (AFs) chemically treated by two methods and coated with multiwall carbon nanotubes (MWCNTs). AFs were treated by two types of acid solutions and coated with oxidized MWCNTs. Scanning electron and atomic force microscopies were conducted to observe the failure modes and correlate the fiber roughness to the IFSS. While both acid treatments caused a small change in fiber roughness, MWCNT deposition largely increased the fiber roughness. The microbond test results indicate that the acid treated fibers exhibited slightly higher IFSS than the untreated fibers and such IFSS is even higher for AFs containing MWCNTs. For chemically treated fibers covered with MWCNTs, a rougher surface with matrix cohesive failure at the edge of the sheared droplet suggests that the IFSS improvement is mainly due to the physicochemical interactions among AF, MWCNT and PP, in addition to mechanical interlocking.

1. Introduction

Multiscale hierarchical composites are a new generation of composite materials comprising a nanometric filler, a micrometric reinforcement (typically a fiber) and a macroscopic matrix consolidating the material [1–3]. Although the nanometric filler may play a variety of roles, it typically enhances a specific property and/or adds multifunctionality to the composite [4–7]. If the filler is electrically conductive, as for the case of carbon nanotubes (CNTs), the resulting multiscale hierarchical composite may have added capabilities such as electromagnetic shielding and self-sensing of strain and damage [8–13]. Several recent works have used the approach of depositing CNTs onto the surface of engineering fibers to manufacture this kind of electro-conductive multiscale composites. Since in this architecture the CNTs are located at the fiber/matrix interface, it has been shown that the interfacial shear strength (IFSS) of the composite is increased by the presence of CNTs, mainly due to increased mechanical interlocking [14–17]. For example, LaBarre et al. [17] deposited multiwall carbon nanotubes (MWCNTs) over Kevlar fibers assisted by N-methylpyrrolidone and found increased pull-out friction for such Kevlar fabrics. However, it is generally accepted that the interfacial strength of a composite has mechanical and chemical components, and the role of the chemical component in multiscale hierarchical composites has been scarcely investigated. Furthermore, the large majority of research works reported to date on multiscale hierarchical composites using CNTs deal with either glass or carbon fibers and a thermosetting polymer [15,18–24], and the use of aramid fibers and thermoplastic polymers have been significantly less investigated [16,25,26]. Aramid fiber (AF)/polypropylene (PP) composites are well known for their high toughness, which makes them especially suitable for impact loading scenarios [27]. However, the IFSS of AF/PP composites is frequently weak, and chemical treatments to the AF have been attempted to address this issue. Among the fiber chemical modifications reported in the literature to improve the adhesion between AFs and different polymer matrices are the treatments based on acids, chlorides, fluorinations and plasma treatments [28–31], where the selection of a specific treatment depends strongly on the polymer matrix to be used. For the most common case of epoxy matrices, amine and oxygen plasma treatments [32], as well as

* Corresponding author.
E-mail address: jorge.uribe@cicy.mx (J. Uribe-Calderon).

http://dx.doi.org/10.1016/j.compositesb.2017.04.006
1359-8368/

treatments with phosphoric acids [33] and chlorides [29] have been reported. The use of methacryloyl chloride in wet surface treatments has been reported to improve the compatibility with polymer matrices such as epoxy [29], unsaturated polyesters [34] and polyethylene [28]. Significantly less work has been reported for the AF/PP material system, where fluorination seems to be the major surface treatment attempted to date for this material system [25]. Kevlar has been used to coat CNTs [35], but this procedure is challenging and does not benefit from the mechanical properties of aramid fibers for composites. Very few research efforts have been conducted to modify aramid fibers [25,28] to further include these CNT-modified AFs into advanced polymer composites. Advanced composites subjected to important mechanical loadings need to include a continuous fiber such as the aramid one, and the presence of carbon nanotubes at their interface may not only improve their IFSS, but also allows structural health monitoring through their electrical conductivity. Therefore, in the present research work, the microbond test was used to examine the interfacial shear strength of AF/MWCNT/PP multiscale composites prepared with AF fibers chemically treated by two methods and coated with MWCNTs. Scanning electron microscopy (SEM), and atomic force microscopy (AFM) are also conducted to correlate the fiber roughness to the measured IFSS of the composite. The fiber surface treatments and the presence of CNTs at the interface modify the interfacial properties of the composites, and the main aim of this work is to evaluate their effect and investigated the chemical and mechanical contributions.

2. Experimental

2.1. Materials

The Twaron Aramid fibers (TF) used were provided by Teijin Aramid Inc. (Emmen, The Netherlands). According to the manufacturer, the fiber elastic modulus ranges from 130 to 180 GPa, the density is 1.45 g/cm^3 and the diameter of a single filament is ~12 μm. The Twaron yarn is composed of approximately 1000 individual filaments. Commercial MWCNTs (Cheaptubes Inc., Vermont, USA) with a length ranging from 1 to 6 μm, internal diameter 5–15 nm and the external diameter 30–50 nm were used.

2.2. Surface treatments

2.2.1. MWCNT oxidation

MWCNTs were chemically oxidized with a 3.0 M solution of an equimolar mixture of nitric and sulfuric acids following the procedure reported in the literature [36]. Briefly, 0.3 g of MWCNTs were mechanically stirred with 70 mL acid solution in a hot plate for 15 min at ~60 °C. The dispersion was sonicated in an ultrasonic bath (70 W, 42 kHz) for 2 h, and then filtered and thoroughly washed with distilled water. Finally, the slurry was dried in a convection oven at 100 °C during 24 h.

2.2.2. Fiber surface treatments

Prior to TF surface modifications, the commercial fiber surface coating (sizing) was removed by a sequential Soxhlet extraction with chloroform, ethanol, acetone, and methanol, as reported elsewhere [37]. The extraction time was 6 h for each solvent followed by overnight drying at 70 °C in a convection oven. Two chemical treatments were carried out on the TF after sizing remotion, one (aggressive) based on a mixture of nitric and sulfuric acids, and a (milder) second one based on a solution of chlorosulfonic acid in dichloromethane, as described elsewhere [38]. The first treatment was performed by immersing the TF yarn free of sizing in 490 mL of a 3.0 M mixture of HNO_3 and H_2SO_4 for 1 h. Then, the fibers were washed with 1.5 L of distilled water. For the second treatment, the TFs (free of sizing) were treated with 500 mL of a solution of chlorosulfonic acid in dichloromethane (0.2% w/w) at room temperature for 2 min; then, the TFs were soaked in distilled water for 2 min and finally dried for 1 h at 70 °C. This treatment is expected to generate sulfonic groups (SO_3H) at the fiber surface [38]. The nomenclature used to identify the fibers and their chemical treatments are listed in Table 1.

2.2.3. Surface coating of aramid fibers with carbon nanotubes

As-received and chemically treated aramid fibers were covered with MWCNTs by a immersion coating method assisted by ultrasound, as described elsewhere [38]. Briefly, 4 mg of previously oxidized MWCNTs were deposited onto ~550 mg aramid fibers rolled on a cylindrical frame and immersed into 100 mL of chloroform. The MWCNT deposition onto aramid fibers was conducted by using an ultrasonic horn for 1 h at 165 W and 20 kHz, drying the fibers in a convection oven.

2.3. Fiber roughness and microscopy analysis

The surface topography of the fibers was observed by tapping-mode AFM. Tapping mode, oscillating the tip near its resonance frequency, was preferred for keeping the probe tip close enough to the sample while preventing it from sticking to the surface. The AFM images were recorded with a Bruker SPM8 AFM scanning probe microscope in air at room temperature at a resonant frequency of 320 kHz. Commercially available silicon cantilevers were used (TESP-SS nanoprobe, Bruker) with a cantilever spring constant of 42 N/m, a tip cone angle of 10° and tip radius of about 2 nm, using a scanning frequency of 1 Hz. AFM analysis was conducted over 3 μm by 3 μm sampled areas on the fiber surface. A statistical analysis of 2.5 μm by 2.5 μm central sections of the AFM sampled areas was then carried out. To this aim, the 2.5 μm × 2.5 μm area was divided into 25 sub-areas of 500 nm × 500 nm and the root mean square (RMS) roughness of each sub-area was measured with the Bruker "NanoScope" analysis software. The average and coefficient of variation (CV) of the 40 data were calculated using the RMS roughness of each sub-area as a central metric. For SEM analysis, the AFs were gold-coated and observed using a JEOL JSM-630-LV SEM operated at 20–25 kV.

2.4. Microbond test

Specimens for microbond test consisted of six groups of individual Twaron fibers (as listed in Table 1) containing a PP microdroplet. To this aim, PP powder was previously sieved by using a Tyler # 100 mesh and sprinkled onto the fibers, held by a 15 cm × 8 cm metallic frame. The frame was then heated to 190 °C for 1 h in a vacuum oven (Precision Scientific) to melt the PP powder. Then, the frame was taken off the oven to cool it down to room temperature. Each microdroplet was observed in an optical microscope (Leica DMLM) using transmitted light, 20× objective lens. A picture was captured for each microdroplet, and the

Table 1
Nomenclature of the Twaron fibers and their treatments.

Fiber	Treatment
TF	As-received (untreated) TF.
TFAC	TF modified with 3.0 M mixture of HNO_3 and H_2SO_4.
TFCL	TF modified with chlorosulfonic acid.
TF-MWCNT	As-received TF coated with oxidized MWCNTs.
TFAC-MWCNT	TFAC coated with oxidized MWCNTs.
TFCL-MWCNT	TFCL coated with oxidized MWCNTs.

diameter of the monofilament and the embedded length of each microdroplet was measured using the Image Pro Plus software; only the symmetric microdroplets were selected.

Specimens for the microbond test were prepared by cementing one end of the fiber to a metallic stub; the fiber length between the edge of the stub and the microdoplet was 15 mm. 25 specimens were prepared for each fiber sample. The microbond test was carried out in a microtensometer equipped with a load cell of 50 g and two beveled blades forming a slit, whose gap can be adjusted with a micrometer (Fig. 1). As shown in Fig. 1, the microdroplet was held into the slit, a 10 μm gap was set between the blade tips and the fiber surface, and the metallic stub of the microdroplet was attached to the fixture of the load cell. The crosshead displacement rate was 0.08 mm/s; the microdroplet was pushed against the blades until it was debonded and displaced along the fiber once the shearing force exceeded the interfacial bond strength. The load-displacement curve of each test was recorded and the maximum pull-out force was determined. The IFSS was calculated using the maximum pull-out force (F), the diameter of the monofilament (d), and the embedded length of each droplet (L) as,

$$IFSS = \frac{F}{\pi dL} \quad (1)$$

The debonded surfaces of the tested specimens were observed in a Jeol SEM model JSM 6360LV operated at 20 kV. The sample surfaces were covered with a thin layer of gold for better imaging.

3. Results

3.1. Morphological analysis of the aramid fibers

AFM images of the untreated and treated fibers coated or not with MWCNTs are presented in Fig. 2 and their average RMS roughness and CV are shown in Table 2. The untreated TF (Fig. 2a) has a relatively smooth surface with average surface roughness of 3.2 nm and, according to Table 2, the fibers treated with the mixture of nitric and sulfuric acids (Fig. 2b) and those treated with chlorosulfonic acid (Fig. 2c) present similar surface roughness. The data scattering (CV) of the TF surface is given by the hills and valleys generated by the fiber manufacturing process. The CV of TFAC is significantly higher than that for TF and TFCL, indicating that the aggressive character of the nitric-sulfuric acid treatment caused a non-homogeneous distribution of affected areas on the fiber surface.

Regardless of the fiber treatment, upon deposition of MWCNTs (Fig. 2d and f) the RMS surface roughness increases one order of magnitude. The largest surface roughness is observed for the untreated fiber with deposited MWCNTs (TF-MWCNT), with an average RMS roughness of 21.3 nm. This increased roughness is interpreted as a higher areal density of MWCNTs present on the fiber surface, and suggests that the functional groups of the oxidized MWCNTs interact with the sizing of the TF, as has been previously suggested [39,40]. For the fibers with deposited MWCNTs, the CV may be taken as an indicative of the homogeneity of MWCNT deposition on the fiber surface. The TF-MWCNT surface yields the lowest CV, suggesting that the deposited MWCNTs on TFAC and TFCL is less homogeneous than on the untreated TF. This suggests that the mixture of nitric and sulfuric acids is aggressive with the fiber surface yielding a large density of oxygen-containing functional groups in localized zones of the fiber [41,42]; these groups interact with the functional groups of the oxidized MWCNTs, probably through hydrogen bonding [43]. However, the experimental conditions of the chlorosulfonic acid treatment (although mild) are sufficient to generate a rather homogenous distribution of functional groups on the fiber surface.

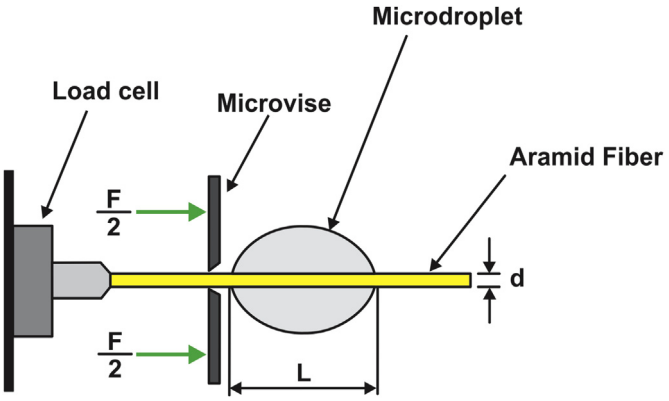

Fig. 1. Experimental setup for the microbond test.

Fig. 3 shows SEM images of as-received, chemically treated, and MWCNT-modified aramid fibers taken at 1000× (scale bar 100 μm) and 5000× (scale bar 5 μm) magnifications. A relatively smooth surface is observed for the as-received fibers (Fig. 3a) with very few shallow surface markings which stem from the fiber manufacturing process. Major fiber damage was not observed among the treated fibers (Fig. 3b and c); nevertheless, some individual fibers treated with the mixture of nitric and sulfuric acids showed an increased surface roughness and peeling off damage (Fig. 3b).

As observed in Fig. 3d and f, the surface of the aramid fibers significantly changes upon MWCNT deposition on the fiber surface, yielding a conspicuous change in their surface morphology and surface roughness. The TF-MWCNT (Fig. 3d) shows a high concentration of MWCNT covering the fiber, concomitant with the high values of RMS roughness described above. The TFAC-MWCNT (Fig. 3e), however, is quite different, with less concentration of MWCNTs over the fibers and more heterogeneously distributed. The TFCL-MWCNT (Fig. 3f) shows also a non-homogeneous distribution of MWCNTs over the fibers surface, with an areal concentration which seems slightly lower than that of TF-MWCNT.

3.2. Interfacial shear strength

Fig. 4 shows the typical load-displacement curves for the debonding process of PP microdroplets deposited on the AFs listed in Table 1. The nomenclature used for the microdoplet specimens is the same as in Table 1 but adding PP to indicate the material of the polymer droplet. It can be seen from the figure that TFAC/PP and TFCL/PP systems require higher shear load to debond the PP droplets than the TF/PP system. It is also noticed that the failure load increases upon MWCNT deposition and fiber surface treatment.

Table 3 summarizes the results from the microbond test. IFSS was calculated from Eq. (1) using the maximum load from the load-displacement curves, the length of PP microdroplets (163–185 μm) and the fiber diameter. TFAC/PP and TFCL/PP show comparable values of IFSS (6.28 and 6.47 MPa, respectively) and higher than that for TF/PP (5.86 MPa). The untreated fiber (TF/PP) showed a limited compatibility with PP and the TF-MWCNT/PP monofilament composite showed higher IFSS than TF/PP; since this fiber was not chemically treated, this indicates that the sole presence of MWCNTs on the fiber surface improves the IFSS, likely because of a mechanical contribution (friction and/or mechanical interlocking). The high surface roughness of TF-MWCNT (21.3 nm, see Table 2) is related to a high density of MWCNTs distributed on the fiber surface, and is expected to play a contributing role on the IFSS. Nevertheless, these morphological advantages are not enough to

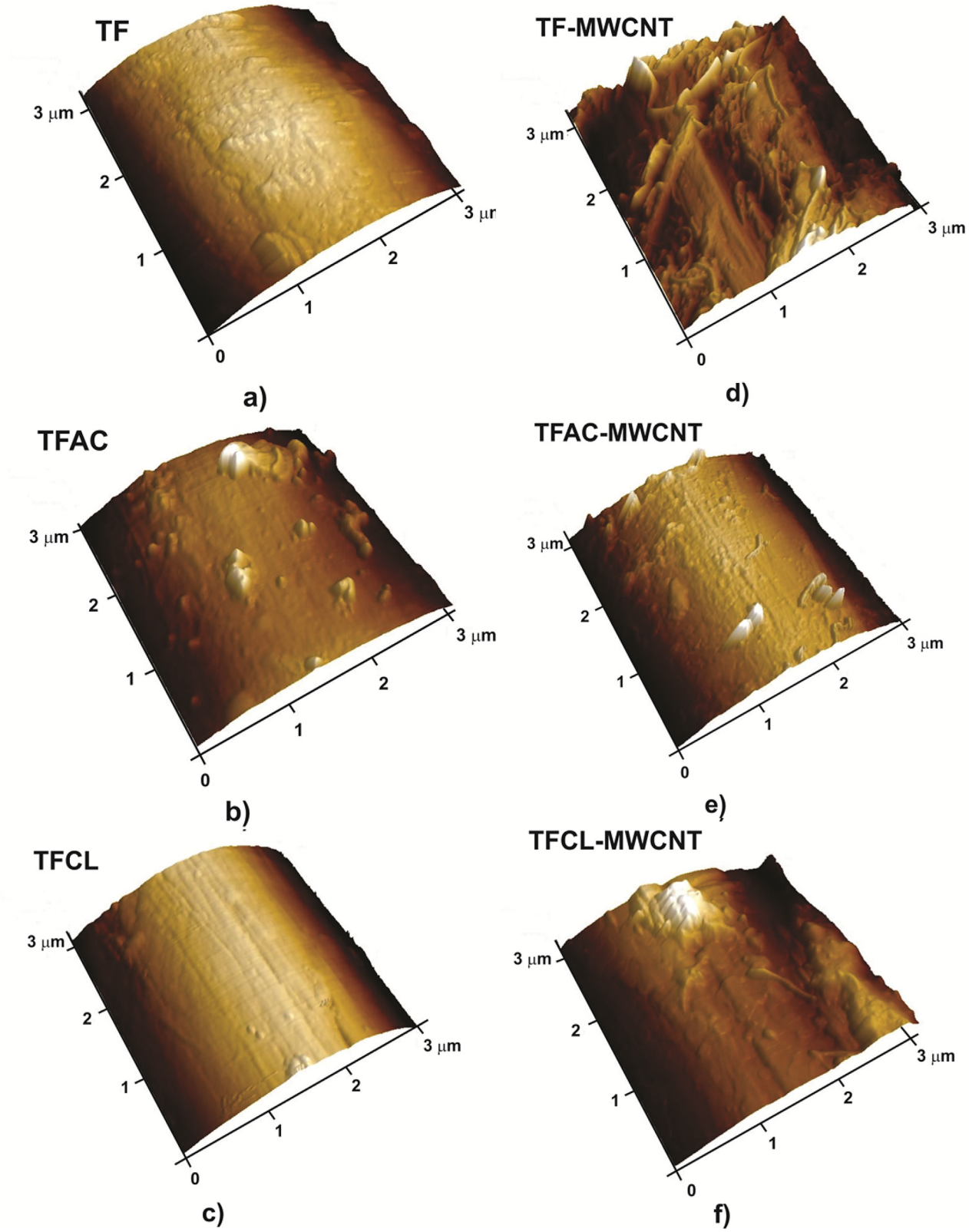

Fig. 2. AFM topographical images of the Twaron fibers. a) TF, b) TFAC, c) TFCL, d) TF-MWCNT, e) TFAC-MWCNT, f) TFCL-MWCNT.

improve the interfacial strength, probably because the MWCNT are only weakly bonded to the fiber surface. The higher concentration of MWCNTs for TF-MWCNT can be explained due to the presence of the surface coating on Twaron fibers. In fact, initial experiments (not reported herein) showed that the MWCNTs do not properly bond to the aramid fiber surface if its sizing is removed and the fiber surface is not chemically activated. The sizing on the fiber surface contains ramifications of ethylene and propylene oxide

Table 2
RMS surface roughness of untreated, chemically treated and MWCNT-modified Twaron fibers.

Statistical metric	Sample					
	TF	TFAC	TFCL	TF-MWCNT	TFAC-MWCNT	TFCL-MWCNT
RMS (nm)	3.2	3.6	3.1	21.3	12.3	11.1
CV	0.34	0.60	0.35	0.32	0.56	0.43

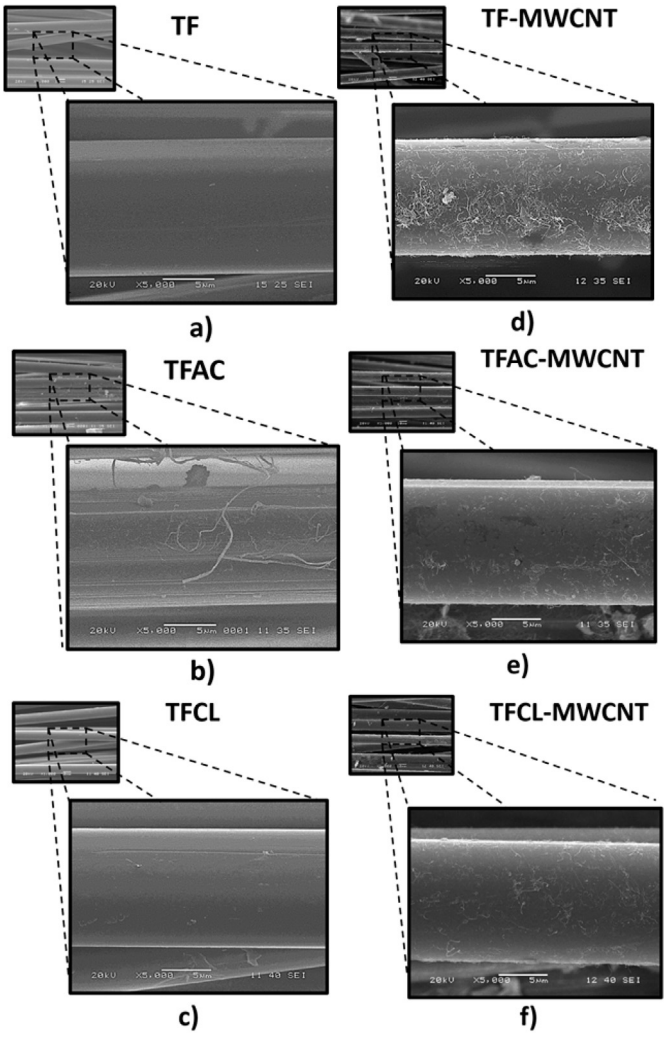

Fig. 3. SEM micrographs of the Twaron fibers. a) TF, b) TFAC, c) TFCL, d) TF-MWCNT, e) TFAC-MWCNT, f) TFCL-MWCNT.

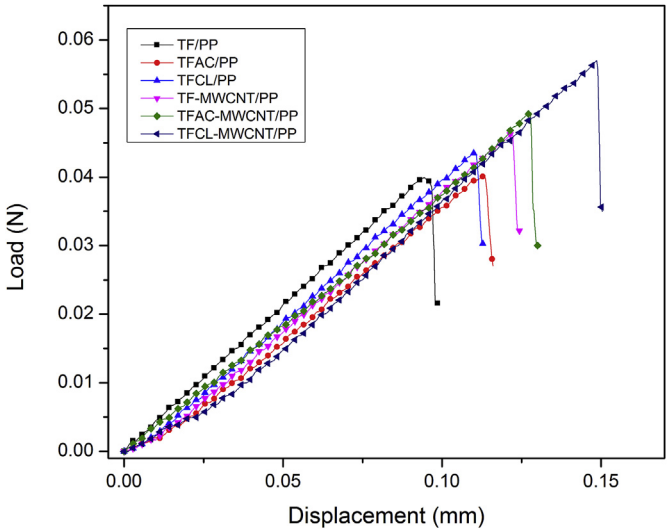

Fig. 4. Representative load-displacement curves for the microbond test of Twaron fiber/PP.

Table 3
IFSS of Twaron/PP with different fiber conditions.

Sample	IFSS (MPa)
TF/PP	5.86 ± 0.49
TFAC/PP	6.28 ± 0.83
TFCL/PP	6.47 ± 1.09
TF-MWCNT/PP	6.79 ± 1.14
TFAC-MWCNT/PP	7.36 ± 0.80
TFCL-MWCNT/PP	8.71 ± 1.54

functional groups, as well as hydroxyl and carboxyl groups [44,45]. Upon ultrasonic MWCNT deposition at ~70 °C, it is possible that the hydroxyl and carboxyl groups of the oxidized MWCNTs react with the ethylene and propylene oxides through anionic ring-opening reaction [39,46,47]; hydrogen bonding is also likely to happen between the OH groups of the fiber sizing and the hydroxyl and/or carboxyl groups on the MWCNT surface [40]. The thickness of the MWCNT layer on the fiber surface has also been recently shown to play a paramount role on the IFSS [48]. For nitric-sulfuric treated fibers, the deposition of MWCNTs produced an increase of IFSS from 6.28 MPa (TFAC/PP) to 7.36 MPa (TFAC-MWCNT/PP). The chlorosulfonic treatment led to the highest IFSS (average of 6.47 MPa) which increased 35% by the MWCNT presence (8.71 MPa).

The increase in IFSS of the MWCNT-coated fibers is not proportional to their large increase in roughness upon MWCNT deposition (Table 2). This means that the increments in IFSS cannot be explained solely by a roughness component, and an important chemical component is contributing to the generation of a stronger interface. The MWCNTs are not bonded to the TF surface but to the sizing which makes them easily peelled off during the microbond test; oxygen-containing species on the surface of TFAC could contribute to the formation of chemical bonds with the MWCNTs, promoting adhesion at the interface and increasing the IFSS. Indeed, XPS results (reported in Ref. [38]) suggested that the TFAC and TFCL present different degrees of oxidation. However, the aggressive acid treatment produced surface damage to fibers, as seen on the SEM micrographs (Fig. 3). The chlorosulfonic treatment has the highest level of IFSS, likely because the interaction of this fiber with the PP droplet has an important chemical component.

To study the failure mechanism caused by the different chemical modifications on the fiber surface and MWCNT deposition, microdroplets were observed by SEM after testing, as shown in Fig. 5; as for most typical microbond tests, the crack initiates due to the localized stress concentrations in the interface, near the region where the microvise edges contact the PP droplet. The crack propagates near the matrix/fiber interface along the loading direction before complete debonding occurs. In the first row, images

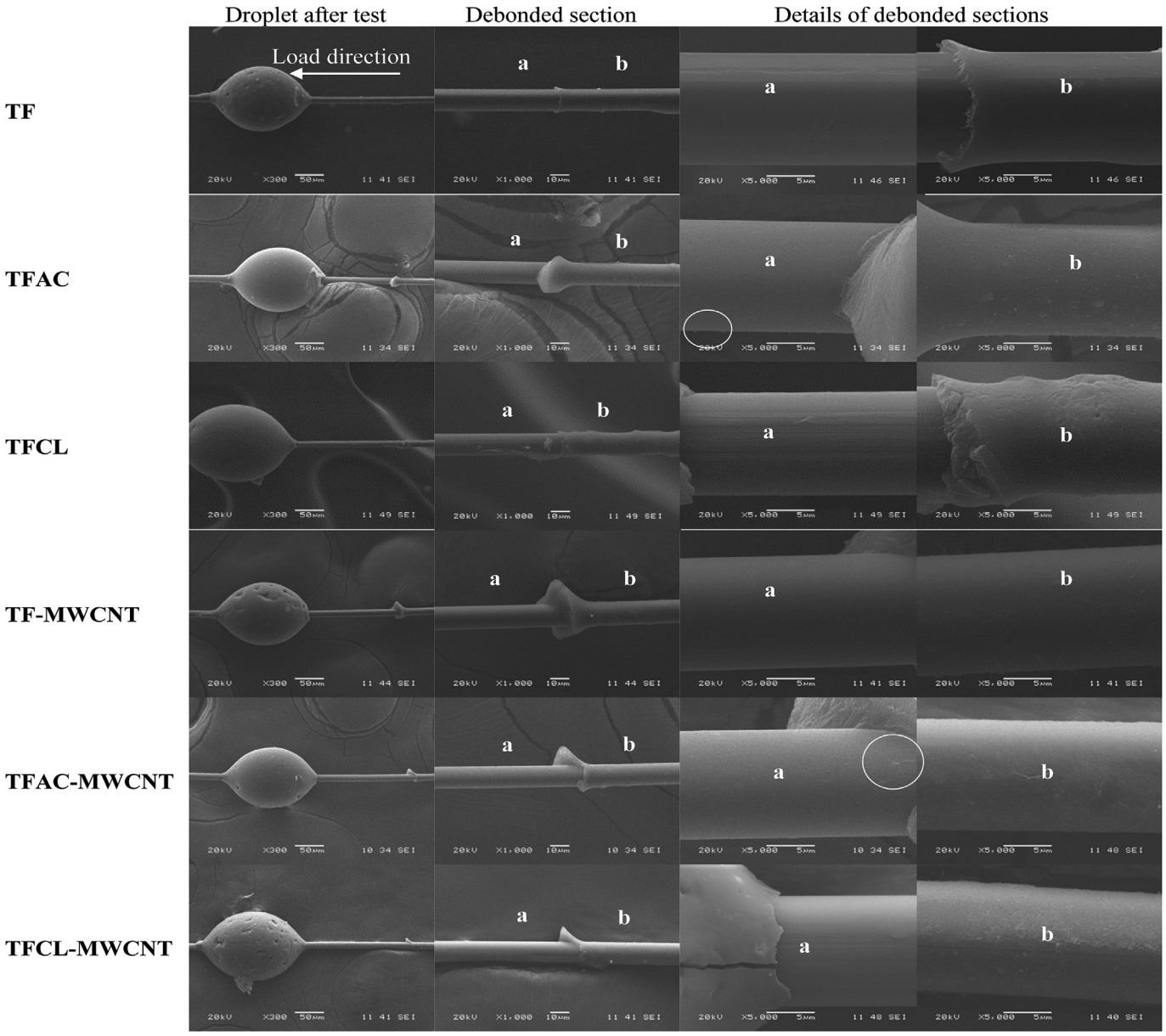

Fig. 5. SEM images of PP microdroplets after the microbond test.

of TF/PP are presented showing a clean interfacial fracture, which is a consequence of the poor TF/PP adhesion (section ***a*** from the debonded section). The debonded surface of TFAC is shown in the second row, where a clean fracture is also observed; however, on the undisturbed fiber surface (section ***b***) some surface irregularities are found (caused by the acid treatment), which may contribute to the increment of IFSS measured. A similar failure mechanism was observed for TFCL (third row), but with a few indications of matrix debris attached to the fiber surface, supporting its increased IFSS. The failure mechanism did not change for TF-MWCNT (fourth row), TFAC-MWCT (fifth row) and TFCL-MWCNT (sixth row), but a few distinctive features can be pinpointed for treated fibers coated with MWCNTs. Although on the fiber fracture surface (debonded section ***a***) no evidence of MWCNT presence was observed, on the undisturbed fiber surface (section ***b***) MWCNTs can be devised, supporting the higher level of IFSS shown. It has been argued that the presence of a CNT layer on the fiber surface yields a stiffness gradient which may diminish the localized stress concentrations. The fact that the MWCNTs are not visible at the debonded sections may indicate that either the crack propagated in a resin rich layer on top of the fiber/matrix interface or the MWCNTs where pulled off during the microbond test. From observations of Fig. 5, the former conclusion seems more viable. Higher improvements may need of chemical treatments that modify the hydrophobicity and/or polarity of the polymer matrix.

4. Conclusions

The influence of two chemical treatments (oxidation by a mixture of nitric/sulfuric acids or a chlorosulfonic acid) and the presence of multiwall carbon nanotubes (MWCNTs) on the surface of aramid fibers (AF) on the interfacial shear strength (IFSS) of AF/MWCNT/PP multiscale composites were evaluated. Both, acid treatments and MWCNT deposition increased the fiber surface roughness, but the effect was significantly larger upon MWCNT deposition. SEM observations revealed that the MWCNT coating

depends on the fiber surface treatment. Higher IFSS was found for treated fibers, regardless of the fiber roughness. The IFSS increased more upon MWCNT deposition on treated fibers, probably because of the stiffness gradient formed at the interface. The results suggest that the higher IFSS observed is mainly due to increased physico-chemical interactions among the AF, MWCNTs and PP upon surface treatments and MWCNT deposition, and that a mechanical contribution exists.

Acknowledgements

This work was supported by CONACYT CIAM project No. 188089 under the direction of Dr. Avilés. Support of CONACYT through project No. 268595 is also acknowledged. The authors would like to thank to Teijin Aramid Inc. for providing the aramid fiber. Technical assistance of Santiago Duarte (CICY) and Patricio Toro (U. Chile) is also strongly appreciated.

References

[1] Quian H, Greenhalgh ES, Shaffer MSP, Bismarck A. Carbon nanotube-based hierarchical composites: a review. J Mater Chem 2010;20:4751–62.
[2] Wang Y, Xu Z, Chen L, Jiao Y, Wu X. Multi-scale hybrid composites-based carbon nanotubes. Polym Compos 2011;32:159–67.
[3] Wang BC, Zhou X, Ma KM. Fabrication and properties of CNTs/carbon fabric hybrid multiscale composites processed via resin transfer molding technique. Compos Part B-Eng 2013;46:123–9.
[4] Kang I, Heung YY, Kim JH, Lee JW, Gollapudi R, Subramaniam S, et al. Introduction to carbon nanotube and nanofiber smart materials. Compos Part B-Eng 2006;37:382–94.
[5] Castano LM, Flatau AB. Smart fabric sensors and e-textile technologies: a review. Smart Mater Struct 2014;23. 053001 (27 pp).
[6] Kundalwal SI, Ray MC. Effect of carbon nanotube waviness on the effective thermoelastic properties of a novel continuous fuzzy fiber reinforced composite. Compos Part B 2014;57:199–209.
[7] Zhou HW, Mishnaevsky Jr L, Yi HY, Liu YQ, Hu X, Warrier A, et al. Carbon fiber/carbon nanotube reinforced hierarchical composites: effect of CNT distribution on shearing strength. Compos Part B Eng 2016;88:201–11.
[8] Liu Y, Song D, Wu C, Leng J. EMI shielding performance of nanocomposites with MWCNTs,nanosized Fe_3O_4 and Fe. Compos Part B-Eng 2014;63:34–40.
[9] Monti M, Natali M, Petrucci R, Kenny JM, Torre L. Carbon nanofibers for strain and impact damage sensing in glass fiber reinforced composites based on an unsaturated polyester resin. Polym Compos 2011;32:766–75.
[10] An Q, Rider AN, Thostenson ET. Hierarchical composite structures prepared by electrophoretic deposition of carbon nanotubes onto glass fibers. Appl Mater Interfaces 2013;5:2022–32.
[11] Abot JL, Song Y, Sri Vatsavaya M, Medikonda S, Kier Z, Jayasinghe C, et al. Delamination detection with carbon nanotube thread in self-sensing composite materials. Compos Sci Technol 2010;70:1113–9.
[12] Baltopoulos A, Polydorides N, Pambaguian L, Vavouliotis A, Kostopoulos V. Exploiting carbon nanotube networks for damage assessment of fiber reinforced composites. Compos Part B-Eng 2015;76:149–58.
[13] Kim H. Enhanced crack detection sensitivity of carbon fiber composites by carbon nanotubes directly grown on carbon fibers. Compos Part B 2014;60:284–91.
[14] Godara A, Gorbatikh L, Kalinka G, Warrier A, Rochez O, Mezzo L, et al. Interfacial shear strength of a glass fiber/epoxy bonding in composites modified with carbon nanotubes. Compos Sci Technol 2010;70:1346–52.
[15] Yu B, Jiang Z, Tang X-Z, Yue CY, Yang J. Enhanced interphase between epoxy matrix and carbon fiber with carbon nanotube-modified silane coating. Compos Sci Technol 2014;99:131–40.
[16] Zhang L, Su D, Jin L, Li C. Polyamide 6 composites reinforced with glass fibers modified with electrostatically assembled multiwall carbon nanotubes. J Mater Sci 2012;47:5446–54.
[17] LaBarre ED, Calderon-Colon X, Morris M, Tiffany J, Wetzel E, Merkle A, et al. Effect of a carbon nanotube coating on friction and impact performance of kevlar. J Mater Sci 2015;50(16):5431–42.
[18] Warrier A, Godara A, Rochez O, Mezzo L, Luizi F, Gorbatikh L, et al. The effect of adding carbon nanotubes to glass/epoxy composites in the fibre sizing and/or the matrix. Compos part A-Appl S 2010;41:532–8.
[19] Wicks SS, de Villoria RG, Wardle BL. Interlaminar and intralaminar reinforcement of composite laminates with aligned carbon nanotubes. Compos Sci Technol 2010;70:20–8.
[20] Sui X, Shi J, Yao H, Xu Z, Chen L, Li X, et al. Interfacial and fatigue-resistant synergetic enhancement of carbon fiber/epoxy hierarchical composites via an electrophoresis deposited carbon nanotube-toughened transition layer. Compos Part A Appl Sci Manuf 2017;92:134–44.
[21] Wu G, Ma L, Liu L, Wang Y, Xie F, Zhong Z, et al. Interfacially reinforced methylphenylsilicone resin composites by chemically grafting multiwall carbon nanotubes onto carbon fibers. Compos Part B-Eng 2015;82:50–8.
[22] Lee SO, Choi SH, Kwon SH, Rhee KY, Park SJ. Modification of surface functionality of multi-walled carbon nanotubes on fracture toughness of basalt fiber-reinforced composites. Compos Part B-Eng 2015;79:47–52.
[23] Boddu VM, Brenner MW, Patel JS, Kumar A, Mantena PR, Tadepalli T, et al. Energy dissipation and high-strain rate dynamic response of E-glass fiber composites with anchored carbon nanotubes. Compos Part B-Eng 2016;88:44–54.
[24] Dai G, Mishnaevsky Jr L. Carbon nanotube reinforced hybrid composites: computational modeling of environmental fatigue and usability for wind blades. Compos Part B-Eng 2015;78:349–60.
[25] O'Connor I, Hayden H, Coleman JN, Gun'ko YK. High-strength, high-toughness composite fibers by swelling kevlar in nanotube suspensions. Small 2009;5:466–9.
[26] Chen W, Qian X-M, He X-Q, Liu Z-Y, Liu J-P. Surface modification of kevlar by grafting carbon nanotubes. J Appl Polym Sci 2012;123:1983–90.
[27] Bazhenov Z. Dissipation of energy by bulletproof aramid fabric. J Mater Sci 1997;32:4167–73.
[28] Petsalas HJ, Andreopoulos AG. Treated aramid fibers as reinforcement in nonpolar matrices. J Appl Polym Sci 1989;38:593–604.
[29] Tarantili PA, Andreopoulos AG. Mechanical properties of epoxies reinforced with chloride-treated aramid fibers. J Appl Polym Sci 1997;65:267–76.
[30] Maity J, Jacob C, Das CK, Kharitonov AP, Singh RP, Alam S. Fluorinated aramid fiber reinforced polypropylene composites and their characterization. Polym Compos 2007;28:462–9.
[31] Jia C, Chen P, Li B, Wang Q, Lu C, Yu Q. Effects of twaron fiber surface treatment by air dielectric barrier discharge plasma on the interfacial adhesion in fiber reinforced composites. Surf Coat Tech 2010;204:3668–75.
[32] Jang BZ. Control of interfacial adhesion in continuous carbon and kevlar fiber reinforced polymer composites. Compos Sci Technol 1992;44:333–49.
[33] Li G, Zhang C, Wang Y, Li P, Yu Y, Jia X, et al. Interface correlation and toughness matching of phosphoric acid functionalized kevlar fiber and epoxy matrix for filament winding composites. Compos Sci Technol 2008;68:3208–14.
[34] Andreopoulos AG. A new coupling agent for aramid fibers. J Appl Polym Sci 1989;38:1053–64.
[35] O'Connor I, Hayden H, O'Connor S, Coleman JN, Gun'ko YK. Polymer reinforcement with kevlar-coated carbon nanotubes. J Phys Chem C 2009;113:20184–92.
[36] Avilés F, Cauich-Rodríguez JV, Moo-Tah L, May-Pat A, Vargas-Coronado R. Evaluation of mild acid oxidation treatments for MWCNT functionalization. Carbon 2009;47:2970–5.
[37] Lin T, Wu S, Lai J, Shyu S. The effect of chemical treatment on reinforcement/matrix interaction in kevlar-fiber/bismaleimide composites. Compos Sci Techno 2000;60:1873–8.
[38] Rodríguez-Uicab O, Avilés F, Gonzalez-Chi PI, Canché-Escamilla G, Duarte-Aranda S, Yazdani-Pedram M, et al. Deposition of carbon nanotubes onto aramid fibers using as-received and chemically modified fibers. Appl Surf Sci 2016;385:379–90.
[39] Li M, Gu Y, Liu Y, Li Y, Zhang Z. Interfacial improvement of carbon fiber/epoxy composites using a simple process for depositing commercially functionalized carbon nanotubes on the fibers. Carbon 2013;52:109–21.
[40] Ku-Herrera JJ, Avilés F, Nistal A, Cauich-Rodríguez JV, Rubio F, Rubio J, et al. Interactions between the glass fiber coating and oxidized carbon nanotubes. Appl Surf Sci 2015;330:383–92.
[41] Chatzi E, Koenig J. Morphology and structure of kevlar fibers: a review. Polym-Plast Technol 1987;26:229–70.
[42] Uppal R, Ramaswamy GN, Loughin T. A novel method to assess degree of crystallinity of aramid filament yarns. J Ind Text 2012;43:3–19.
[43] O'Connor I, Hayden H, O'Connor S, Coleman JN, Gun'ko YK. Kevlar coated carbon nanotubes for reinforcement of polyvinylchloride. J Mater Chem 2008;18:5585–8.
[44] De Lange P, Akker P, Maas A, Knoester A, Brongersma H. Adhesion activation of Twaron® aramid fibres studied with low-energy ion scattering and x-ray photoelectron spectroscopy. Surf Interface Anal 2001;31:1079–84.
[45] De Lange PJ, Mäder E, Mai K, Young RJ, Ahmad I. Characterization and micromechanical testing of the interphase of aramid-reinforced epoxy composites. Compos Part A-Appl S 2001;32:331–42.
[46] Thompson MS, Vadala TP, Vadala ML, Lin Y, Riffle JS. Synthesis and applications of heterobifunctional poly(ethylene oxide) oligomers. Polymer 2008;49:345–73.
[47] Blank W, He ZA, Picci M. Catalysis of the epoxy-carboxyl reaction. J Coatings Technol 2002;74:33–41.
[48] Tamrakar S, An Q, Thostenson ET, Rider AN, Haque BZ, Gillespie Jr JW. Tailoring interfacial properties by controlling carbon nanotube coating thickness on glass fibers using electrophoretic deposition. ACS Appl Mater Interfaces 2016;8:1501–10.